Composites Science and Technology 207 (2021) 108731

Contents lists available at ScienceDirect

Composites Science and Technology

journal homepage: http://www.elsevier.com/locate/compscitech

Co/multi-walled carbon nanotubes/polyethylene composites for microwave absorption: Tuning the effectiveness of electromagnetic shielding by varying the components ratio

Mariya A. Kazakova [a,*], Nina V. Semikolenova [a], Evgeniy Yu. Korovin [b], Viktor A. Zhuravlev [b], Alexander G. Selyutin [a], Dmitry A. Velikanov [c], Sergey I. Moseenkov [a], Andrey S. Andreev [d], Olga B. Lapina [a], Valentin I. Suslyaev [b], Mikhail A. Matsko [a], Vladimir A. Zakharov [a], Jean-Baptiste d'Espinose de Lacaillerie [e]

[a] Boreskov Institute of Catalysis, SB RAS, Lavrentieva 5, Novosibirsk, 630090, Russia
[b] National Research Tomsk State University, Lenin Ave. 36, Tomsk, 634050, Russia
[c] Kirensky Institute of Physics, SB RAS, Akademgorodok St. 50, Krasnoyarsk, 660036, Russia
[d] TOTAL Research and Technology Feluy (TRTF), Zone Industrielle C, 7181, Feluy, Belgium
[e] Soft Matter Science and Engineering (SIMM), UMR CNRS 7615, ESPCI Paris, Université PSL, Sorbonne Université, 75005, Paris, France

ARTICLE INFO

Keywords:
Polymer composites
Multi-walled carbon nanotubes
Co nanoparticles
Hybrid structures
Electromagnetic interference shielding

ABSTRACT

We present novel polyethylene (PE) composites for electromagnetic interference (EMI) shielding application. They are based on cobalt modified multi-walled carbon nanotubes (MWCNTs) produced via *in situ* polymerization of ethylene, with the Ti-Ziegler–Natta catalyst preliminarily immobilized on Co/MWCNT hybrids. The electromagnetic properties of the composites were tuned by varying the filler loading and Co:MWCNT ratio. The microstructure of the composites and electromagnetic absorption process were carefully characterized by transmission and scanning electron microscopy, X-ray diffraction, vibrating sample magnetometry, ferromagnetic resonance and vector network analysis. The electromagnetic wave absorbing properties of the nanocomposite were investigated in the 10 MHz–18 GHz frequency range revealing that the EMI absorption properties can be tuned by varying the Co:MWCNT weight ratio in the filler. Interestingly, the Co/MWCNT-PE composite with a total filler and Co loading of only 12 and 1.7 wt%, respectively, showed extremely high reflection loss (RL) of −55 dB. More importantly, an effective bandwidth of 12.8–17.8 GHz (RL below −10 dB) was achieved for a matching thickness of only 1.5 mm. The specific RL value (RL/filler loading) of the composite was superior in comparison with the previously reported nanostructured carbon materials. The highly effective absorbing properties of Co/MWCNT-PE composites are explained primarily by the unprecedented uniform filler distribution in the polyethylene as well as by the synergistic effect of MWCNTs and Co nanoparticles. This approach thus offered an effective strategy to design cost-effective, lightweight and flexible EMI shielding materials with tunable dielectric and magnetic performance.

1. Introduction

The rapid rise of modern electronic equipment and communication technology has strongly advanced the diffusion of miniature devices in the consumer environment and their multiplication has been a significant source of electromagnetic interference (EMI). Strong EMI pollution is thus a current concern as it can cause the malfunction of various electronic devices in civil, scientific and military applications, and ultimately provoke adverse effects on human health [1]. In this context, carbon polymer composites are extensively studied as lightweight flexible coating materials for electromagnetic shielding [2–6]. The dispersion of conductive carbon particles within a thin flexible dielectric polymer matrix confers to the composite tunable electromagnetic responses that are both practically relevant and theoretically challenging. In most cases, to minimize reflection by impedance matching and enhance adsorption losses, ferromagnetic particles are also dispersed

* Corresponding author.
E-mail address: mas@catalysis.ru (M.A. Kazakova).

https://doi.org/10.1016/j.compscitech.2021.108731
Received 22 October 2020; Received in revised form 18 January 2021; Accepted 15 February 2021
Available online 18 February 2021

within the composite together with the carbon particles [7,8]. In theory, the targeted reflection loss and bandwidth can then be attained for loadings as low as 1 wt% (close to the 3D percolation threshold) when using high aspect ratio carbon particles such as carbon nanotubes (CNT) [9]. In practice however, the dispersion of the CNT is far from ideal. Aggregation or bundling results in performances degraded from the prediction of percolation theory and loading in the range of 30–40 wt% are actually commonly needed [10]. So far, this limitation has been circumvented by designing complex heterogeneous structures such as foams [11,12], aerogels [13–15], and sponges [16]. Another successful strategy has been the inclusion of conductive micrometric needles [17]. However, the complexity and fragility of these materials makes them largely impractical in many cases. In summary, despite the attractive potential of carbon nanotube polymer composites for electromagnetic shielding, it must be recognized that their design and realization remain a challenge.

Recently, we have shown that immobilization of Ti-Ziegler-Natta catalysts on multi-walled CNT (MWCNT) allows the *in situ* polymerization of polyethylene (PE) resulting in a composite with an unprecedented level of dispersion [18–20]. The rationale is that the MWCNT acts as nucleating agent for PE crystallization and template for chain orientation. Independently, we have also investigated the relatively simple deposition of Co metal nanoparticles on MWCNT by incipient wetness impregnation [21,22]. Building on these studies, we show here that a combination of Co deposition on MWCNT and *in situ* polyethylene polymerization provides a new route to synthesize tunable, thin, low-density electromagnetic shielding materials in the 2–18 GHz range. This relies on the fact that Co nanoparticles enhance electromagnetic wave attenuation and are an efficient and versatile efficient absorbing material due to their strong exchange force, controllable crystal structure, and tunable magnetic properties [23,24]. Indeed, investigations of the electromagnetic absorbing properties of the Co/MWCNT-PE composites revealed that EMI absorption properties can be tuned by varying the Co:MWCNT weight ratio in the composite. The best reflection loss, -55 dB at 5.2 GHz, was achieved with a total filler loading as low as 12 wt %, and a Co nanoparticle loading of only 1.7 wt% (thickness of 4 mm). An effective bandwidth 12.8–17.8 GHz (RL below −10 dB) was obtained for a relatively thin value of matched thickness (1.5 mm). To the best of our knowledge, this material had the highest specific reflection losses (SRL = RL/filler loading and SRL = RL/magnetic nanoparticle loading) among previously reported absorbers composites based on commercially available polymer and containing nanostructured carbon materials with magnetic nanoparticles.

2. Material and methods

2.1. Synthesis, post-treatment and functionalization of MWCNTs

The MWCNTs used in this work were synthesized by chemical vapor deposition (CVD) of ethylene gas over bimetallic Fe-Co catalysts at 680 °C [25]. The obtained nanotubes had an average outer diameter of 9.4 nm. After the growth the MWCNT were purified from remaining catalyst particles by boiling in a solution of hydrochloric acid as described in Ref. [26]. Subsequently, the MWCNT were mildly oxidized in concentrated HNO_3 for 120 min to obtain functionalized nanotubes with about 2.4 carboxylic groups per nm^2, a surface area of 260 $m^2\ g^{-1}$ and a purity above 99% [26].

2.2. Co/MWCNT hybrids preparation

Co-containing samples were prepared by incipient wetness impregnation (IWI) of MWCNTs with aqueous solutions of cobalt nitrate ($Co(NO_3)_2{\cdot}6H_2O$, 98%, Sigma-Aldrich) [27]. The concentration of Co nitrates in the impregnation solutions was varied to obtain Co/MWCNT samples containing different Co loading at about 3.5–14.5 wt%. The higher Co content (28–34 wt%) were synthesized by multiple IWI (4 and 5 times) of the 7.5 wt% Co/MWCNT sample. In this case, after each impregnation, the samples were dried at 110 °C and re-impregnated to obtain the desired Co loading in the samples. Fig. 1 displays the scheme of Co/MWCNT hybrids preparation.

Then, a portion of the multistage IWI calcined sample was loaded into a flow-through glass reactor and kept in an argon stream (60 $mL{\cdot}min^{-1}$) for 5 min. After that, argon was replaced by hydrogen (flow rate 50 $mL{\cdot}min^{-1}$), and the sample was heated in the hydrogen stream to 400 °C at a rate of 3 $°C{\cdot}min^{-1}$ and kept at 400 °C for 4 h. After cooling, the reduced sample was purged with argon for 20 min and transferred into glass ampoules, which were sealed without contact with air immediately after the reduction procedure. The exact Co content was determined by X-ray fluorescence (XRF) using a sequential spectrometer ARL Perform'X with a Rh anode X-ray tube according to Ref. [28]. The prepared samples were denoted as x% Co/MWCNT-Ox, the number x standing for the cobalt load in wt.%.

2.3. Preparation of catalytic systems Co/MWCNT/TIBA/$TiCl_4$ and synthesis of Co/MWCNT-PE composite materials by in situ polymerization

For synthesis of Co/MWCNT-PE composite materials, an *in situ* polymerization technique was chosen. It relies on a previous adsorption of Ti-containing polymerization catalysts on the surface of Co/MWCNTs systems followed by polymerization of ethylene. Fig. 2 displays the scheme of preparation of Co/MWCNT-PE with *in situ* polymerization.

All manipulations were carried out under argon atmosphere using standard Schlenk techniques. A sample of reduced Co/MWCNT (with different Co content 3.5–34 wt%, 1 g) in the argon stream was transferred into the 0.4 L glass reactor and 50–100 mL of heptane was introduced. Further, a solution of triisobutylaluminium (TIBA) in heptane (0.8 mmol per gram of Co/MWCNT) was added. The batch was vigorously stirred at room temperature for 1 h and then left standing for 12 h. After 12 h, the liquid phase was decanted in argon atmosphere through a siphon, and the precipitate formed was washed twice with pure heptane. 50 mL of heptane was added to the washed Co/MWCNT/TIBA sample and a solution of $TiCl_4$ in heptane (0.4 mmol Ti per gram MWCNT) was added with vigorous stirring. The mixture was stirred at room temperature for 30 min, after which the precipitate was allowed to settle and washed twice with pure heptane. Using atomic emission spectroscopy with inductively coupled plasma, the average composition of the obtained Co/MWCNT/TIBA/$TiCl_4$ catalysts was determined to be 0.4 wt% Al and 1.1 wt% Ti. Then, a portion of heptane was added to the catalyst to fill the total volume of 250 mL and the catalyst was dispersed in an ultrasonic bath for 30 min to form a stable suspension. Further the catalyst suspension under argon was transferred into a 1 L steel polymerization reactor preliminarily dried by evacuation at 80 °C. The reactor was charged with 1.4 mmol of cocatalyst (triethylaluminum (TEA)), heated up to 70 °C and saturated with ethylene (4 atm). During the reaction the temperature and the ethylene pressure were maintained constant through an automated ethylene feed which also recorded the ethylene consumption with time.

The polymerization reaction was stopped when the required amount of ethylene, corresponding to the target of about 10 wt% Co/MWCNT additive in the polymer, was reached. The resulting composite materials were separated from the reaction medium, washed with heptane, ethanol, and dried to constant weight. The composites are labeled y% (x % Co/MWCNT)-PE where the first percentage *y* refers to the inorganic (Co/MWCNT) weight fraction and the second one *x* to the Co to MWCNT weight fraction (as in section 2.2). Note that the percent Co weight fraction in the sample is thus *xy*/100.

2.4. Characterization of Co/MWCNT hybrids and Co/MWCNT-PE composite materials

2.4.1. Transmission electron microscopy (TEM)

Morphologies of the Co/MWCNT hybrids and uniformity of the Co/

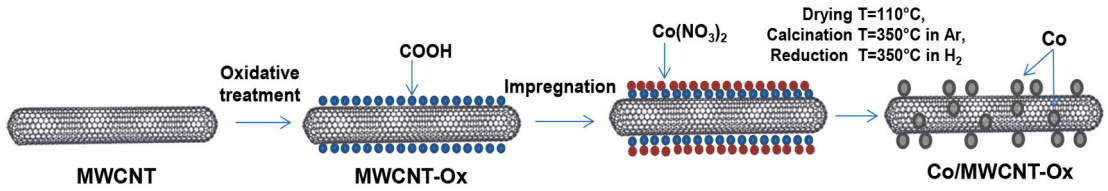

Fig. 1. Scheme of Co/MWCNT hybrid preparation via IWI technique.

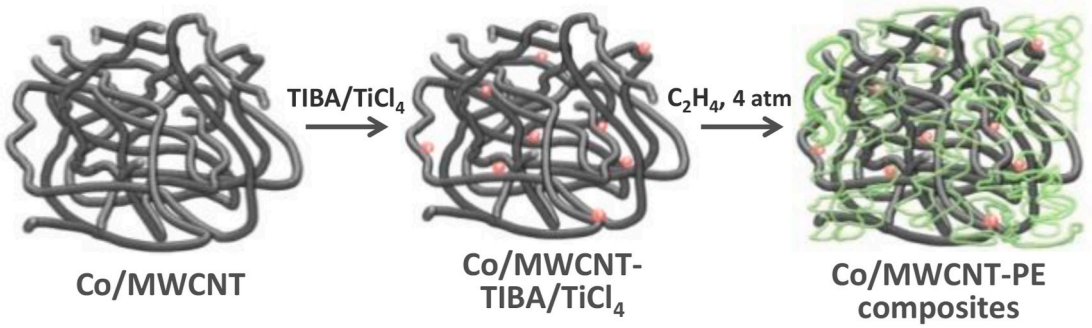

Fig. 2. Scheme of Co/MWCNT-PE composites preparation via *in situ* polymerization.

MWCNT distribution in the polyethylene matrix were characterized by TEM using a JEOL JEM-2010 microscope. It operates at a 200 kV accelerating voltage which allows a nominal resolution of 1.4 Å. Co particle size distributions in the Co/MWCNT samples were estimated by analysis of TEM images containing about 200–400 Co particles at magnifications of × 50 000 and × 400 000. The dimension was measured for Co particles distinguishing those located on the outer surface of the MWCNT and those in their internal channels. Concerning the Co/MWCNT-PE composites, the powder samples were placed onto TEM sample support meshes with an amorphous carbon conducting layer.

2.4.2. Scanning electron microscopy (SEM)

The morphology and structure of the Co/MWCNT-PE composites were investigated by SEM using a JSM6460LV JEOL microscope with an accelerating voltage of 25 kV. For SEM studies, composite films prepared by hot pressing were used, as described below in section 2.5. They were cut into 8 × 3 × 0.5 mm^3 pieces, and then fixed with silver glue to the copper support with the cut section facing the beam.

2.5. Electrophysical properties of Co/MWCNT-PE composite materials

To study the electrophysical properties of the obtained Co/MWCNT-PE composite materials, films were prepared by pressing the obtained powder using a hand hot-press between two polished steel plates covered with Teflon film and a copper frame with a thickness of 0.5 mm as a spacer.

The electrical conductivity of the Co/MWCNT-PE composite materials was measured using a Keithley 6487 picoammeter/power source with the Keithley 8009 measuring chamber. The specific volume conductivity of the composite materials was measured using the ASTM D257 − 14 standard procedure. The nominal film thickness was 0.5 mm. However, the exact measured thickness varied between 0.49 and 0.58 mm. It what follows, we refer to the nominal thickness of 5 mm but the true measured value was used for calculations.

The room temperature ferromagnetic resonance (FMR) spectra of Co/MWCNT-PE composites was collected on a laboratory-made spectrometer using standard waveguide pass-through in the frequency range of 37–53 GHz. The composite samples were taken as film sections completely overlapping the cross section of the rectangular waveguide with dimensions 5.2 × 2.6 mm^2.

The saturation magnetization of the Co/MWCNT-PE composites was investigated within the magnetizing field range ±20 kOe using a vibration magnetometer fitted with electromagnet designed by Puzei. The measurements were carried at room temperatures on samples in the form of cubes with dimensions of ~3 × 3 × 3 mm^3.

The frequency dependences of the electromagnetic parameters (voltage reflection coefficients *S11* and *S22*, voltage transmission coefficients *S21* and *S12*) of Co/MWCNT-PE composite materials were measured in the frequency interval of 10 MHz–18 GHz using an N5247A vector network analyzer (Agilent Technologies) in an N-type coaxial tract [29,30]. The complex values of the permittivity and permeability were calculated for a flat sample at normal incidence of the electromagnetic wave. Based on the tested data of complex permittivity (ε) and permeability (μ) at the given frequency and thickness, the reflection loss (RL) was calculated according to the following Eq. (1) and (2):

$$Z_{in} = \sqrt{\frac{\mu_0\mu_r}{\varepsilon_0\varepsilon_r}}\tan\left(j\left(\frac{2\pi}{c}\right)fd\sqrt{\mu_r\varepsilon_r}\right) \quad (1)$$

$$RL = 20\log|(Z_{in} - Z_0)\,/\,(Z_{in} + Z_0)| \quad (2)$$

where Z_0 is the intrinsic impedance of free space, Z_{in} is the input impedance of the absorber, c is the velocity of the EM wave in air, f is the frequency of the EM wave, and d is the thickness of the absorber. The *RL* was calculated for composites located on conducting metal surface.

3. Results

3.1. Characterization of Co/MWCNT hybrids

As stated in the experimental section, the cobalt localization and MWCNT morphology in the Co/MWCNT hybrids have been examined prior to PE polymerization using TEM at different magnifications. TEM images of reduced Co/MWCNTs samples of different Co content are given in the supplementary data (Fig. S1 a-e). Analysis of the TEM images revealed a dependence of the localization and nanoparticles size on Co loading in line with our previous studies [21,22]. For the samples containing less than 5 wt%, the Co nanoparticles were located exclusively inside the MWCNT (Fig. S1 a) and their size was limited to 4 nm due to internal MWCNT steric constrains. A further increase of Co loading led to a new population of predominantly spherical

nanoparticles on the MWCNT outer surface whose sizes increased with the Co loading, from 14 nm to 45 nm on average (Fig. S1 b-e).

3.2. Optimization of the Co/MWCNT-PE composites preparation

The original magnetic and dielectric properties of Co/MWCNT hybrids can be conserved when they are incorporated as filler in a polymer matrix. However, the main challenge of such composite material production is to prevent oxidation and to achieve a uniform distribution of the filler in the polymer matrix.

As already discussed in our earlier works [21,22], pure Co/MWCNT hybrids are not protected from oxidation by air, and thus their structure cannot be investigated in detail by *ex situ* XRD. XRD patterns were thus acquired *in situ* under a reducing atmosphere to trace the conditions for the formation of Co nanoparticles during reduction and their evolution depending on the reduction temperature. As an example, the dynamics of the formation of Co metal particles and their dimensions have been monitored on the 14.5% Co/MWCNT sample depending on the reduction temperature (Fig. S2). The reduction of Co/MWCNT samples in the temperature range of 140–700 °C in a hydrogen flow results in a phase transition from Co_3O_4 (150–280 °C) through CoO (280–350 °C) to Co (above 350 °C). The size of the coherent domain for all phases of Co remained roughly constant at 15 nm in the reduction temperature range from 140 to 350 °C. Starting at 550 °C, the coherent domain size increased to 30 nm and reached up to 45 nm at the final temperature of 700 °C. Thus, an optimal reduction temperature (350 °C) for the Co/MWCNT samples was determined, making it possible to avoid the sintering process and maintain the minimum size of Co nanoparticles. Consequently, the Co coherent domain size after reduction was 15 nm for 14.5% Co/MWCNT sample, that is a value not far from the initial mean size of the Co particles observed by HRTEM (Fig. S1 c).

Regarding the optimization of dispersion, the Co/MWCNT-PE composites were obtained by *in situ* polymerization. For a better understanding of the influence of polymerization conditions on the uniformity of the distribution of the Co/MWCNT filler in the polyethylene, the polymerization conditions were varied: temperature (70–80 °C), polymerization catalyst ($TiCl_4$) concentration, C_2H_4 pressure (2–4 atm), and H_2 pressure (0–4 atm). The polymer yield decreased when the polymerization temperature increased from 70 to 80 °C, probably because of an associated loss of catalytic sites. The increase in the concentration of the Ti-containing catalyst led to an increase in the total concentration of active catalytic sites and thus to an increase of the polymer yield. Finally, the addition of hydrogen to the polymerization medium favored the hydrogenation of ethylene catalyzed by metallic cobalt particles. Thus, the following polymerization conditions were considered as optimal: polymerization temperature of 70 °C; ethylene pressure of 4 atm; no hydrogen. The polymerization catalysts Co/MWCNT/TIBA/$TiCl_4$ activity data and the composition of the obtained Co/MWCNT-PE composite materials are listed in Table 1. Composite materials MWCNT-PE with different content of MWCNT and without cobalt were also synthesized under similar conditions as reference samples.

From the data in Table 1 it follows that the catalytic systems x% Co/MWCNT/TIBA/$TiCl_4$ (samples #4 to #9) were more active in the polymerization reaction as compared to the corresponding catalysts without Co, MWCNT/TIBA/$TiCl_4$ (samples #1 to #3). This can be explained by a different fixation of the Ti-containing polymerization catalyst on the surface of the Co/MWCNT samples compared to the MWCNT ones.

A tentative explanation based on TEM could be the following. For the MWCNT/TIBA/$TiCl_4$ catalytic system, a thin film enveloping the tubes was observed, revealing a uniform dispersion of the catalytic complex along the MWCNT outer surface (Fig. S3 a-b). However, in the case of catalytic systems containing metallic Co particles, the $TiCl_x$ active sites were located not only on the MWCNT outer surface but also around the Co particles. Polymerization thus proceeded from a larger number of polycrystalline catalytic sites (Fig. S4 a-b) resulting in a higher activity in ethylene polymerization.

Table 1
Catalytic properties of Co/MWCNT/TIBA/$TiCl_4$ and composition of obtained Co/MWCNT-PE composites. Polymerization conditions: cocatalyst TEA (5 ml); polymerization temperature of 70 °C; ethylene pressure of 4 atm. Compositions are in wt.%.

# Samples	x% Co/MWCNT-Ox 1 g	% Ti	Yield of PE g	Activity g PE/(g Ti ·atm·min)	Composition		
					% PE	% Co	% MWCNT
1	MWCNT-Ox	2.2	9.3	3.3	90.3	-	9.7
2	MWCNT-Ox	2.2	8.5	2.6	89.5	-	10.5
3	MWCNT-Ox	1.7	7.7	7.1	88.5	-	11.5
4	3.5% Co/MWCNT	~1	9.7	6.4	90.5	0.3	9.2
5	7.5% Co/MWCNT	~1	10.7	9.9	91.5	0.6	7.9
6	11.5% Co/MWCNT	~1	6.2	15.5	86	1.6	12.4
7	14.5% Co/MWCNT	~1	7.4	16.8	88	1.7	10.3
8	28% Co/MWCNT	~1	9.2	11.5	90	2.8	7.2
9	34% Co/MWCNT	~1	8.3	7.4	89	3.8	7.2

SEM and HRTEM (Fig. 3(b–c) and (d-f), respectively) images of Co/MWCNT-PE composite materials confirm the uniform distribution of all components in polyethylene. According to the analysis of PE reflections, the degree of PE crystallinity for all Co/MWCNT-PE composite was about 60% (Fig. S5). Thus, the introduction of MWCNT and Co/MWCNT into polyethylene does not lead to a significant disordering of its crystal structure.

3.3. Dielectric properties of MWCNT and Co dispersion in Co/MWCNT-PE composites

An initial assessment of the dispersion of the MWCNT and Co/MWCNT filler in the polyethylene composites can be obtained through their static electrical conductivity. When the filler distribution in the polymer matrix is uniform, the electrical conductivity of the composite tends to be higher due to an increased number of electron transfer conductive pathways in the volume of the composite. Fig. 4 is a mapping of the electrical conductivity of the samples according to their Co and MWCNT loading. Considering that the electrical conductivity of neat polyethylene is $\sim 10^{-18}$ S/cm, the electrical conductivity of all the samples was higher by orders of magnitude, ranging from $\sim 10^{-7}$ to 10^{-6} S/cm.

Comparing the series without Co, samples #1 to #3, the conductivity of the MWCNT-PE composites varied only slightly with the MWCNT content, signifying that in the concentration range under study, we were well above percolation threshold. We were not able to prepare samples varying solely in Co concentration but comparing samples at the lower MWCNT content of Fig. 4 map (samples #1, #4, #5, #8 and #9), it was clear that the introduction of cobalt nanoparticles did not lead either to a significant change in the electrical conductivity in the Co/MWCNT-PE composites below a MWCNT content of 10 wt%. However, at higher MWCNT content as in composites samples # 6 and #7, the electrical conductivity significantly increased upon Co deposition. Consequently, composite #6 containing 12.4 wt % MWCNT and 1.6 wt % of Co exhibited the highest electrical conductivity value ($5.3 \cdot 10^{-6}$ S cm^{-1}). It could thus be argued that in these two samples, the metal nanoparticles (being present outside of the MWCNT as spheres of large radius [31], as seen in Figure S1 for loading above 33 wt% per weight of MWCNT)

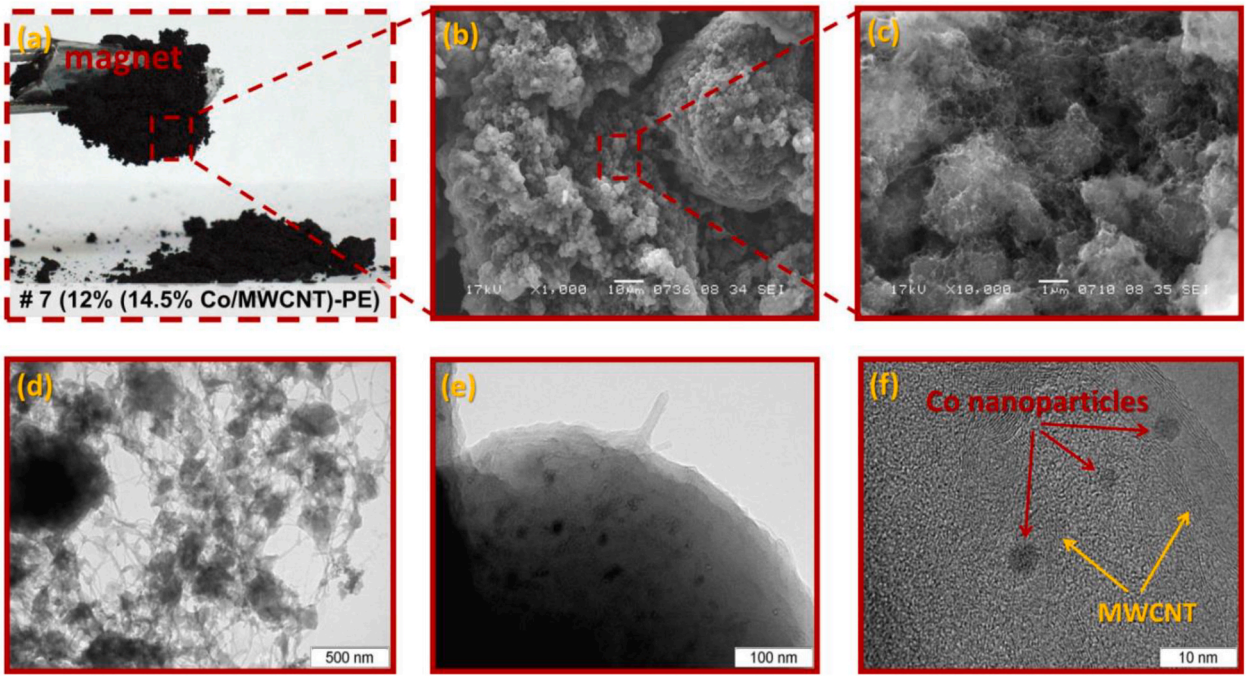

Fig. 3. Morphology and structural characterization of Co/MWCNT-PE composite sample with Co and MWCNT contents of 1.7 and 10.3 wt%, respectively. (a) Digital camera image of as prepared Co/MWCNT-PE composite powder (b-c) Typical SEM and (d-f) TEM images of Co/MWCNT-PE composite sample.

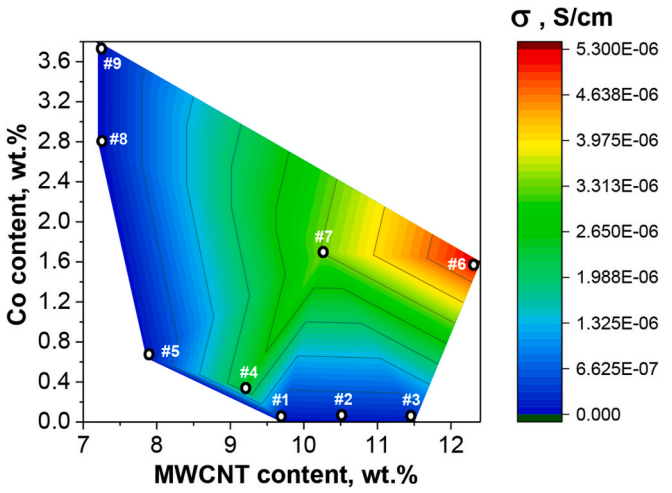

Fig. 4. Static electrical conductivity of Co/MWCNT-PE composites depending on the content of Co and MWCNT in samples, measured at constant field strength (7 V/mm). The thickness of all the samples was about 0.5 mm.

could contribute to the value of static electrical conductivity by decreasing MWCNT junction resistance. The support for this hypothesis is however weakened by the analysis of the frequency dispersion of the conductivity of sample of similar MWCNT content but various Co loading. As seen in Fig. 5, there was no correlation between the conductive behavior and the Co content. However, the AC conductivity (assimilated to the low frequency plateau) increased monotonously with the distance to percolation threshold characterized by the cross-over frequency between the constant and the frequency dependent regimes. This established that the differences in the conductivity were simply related to variations of the MWCNT distribution from one sample to the other.

Nevertheless, while increasing dielectric losses is desired to limit the transmission of the electromagnetic wave through the shielding material, reflection also increases with conductivity. It is thus important to minimize reflection by impedance matching through the magnetic permeability. This is where the Co metal particles are expected to play role.

3.4. Magnetic properties of Co/MWCNT-PE composites

Magnetism is not only an important factor for evaluating the electromagnetic performance but also a way to probe morphology, size, and structure [32]. The magnetic properties of the Co/MWCNT-PE composites have been studied using vibrating sample magnetometer (VSM) at room temperature with maximum applied field of up to ±20 kOe. The B-H magnetic hysteresis loops and magnetic properties for Co/MWCNT-PE composites with various Co:MWCNT:PE ratio are shown in Fig. 6 and Table 2.

Expectedly, the value of magnetization of the Co/MWCNT-PE composites increased with a growth of the Co loading in the samples from 0.3 to 1.7 wt% (Fig. 6). Interestingly, the magnetization curves did not reach saturation even at the maximum probed field of 20 kOe, revealing that the samples were not purely ferromagnetic. The total magnetization could thus be described as the superposition of a para process to the ferro one as in Eq. (3):

$$\sigma_{\Sigma}(H) = \sigma_{\text{ferro}}(H) + \chi_{\text{para}}H \quad (3)$$

where, $\sigma_{ferro}(H)$ is the magnetization of the ferromagnetic phase, which reaches saturation in large fields, $\chi_{para}H$ is the part of the magnetization that grows linearly with the field, and χ_{para} is the susceptibility of the paraprocess.

Regarding the ferromagnetic part of the magnetization/field response, it carried interesting information relative to the Co particle morphologies. Its parameters derived from Fig. 6 are reported in (Table 2). First, the coercive field H_C (field at zero magnetization) increased with the Co particle sizes. In principle, the effective magnetic anisotropy field which determines the coercive force depends on magnetocrystalline anisotropy, shape anisotropy and surface anisotropy but in fact is largely determined by the size of the ferromagnetic particles [33]. Thus the overall magnetic response of the samples confirmed the local HRTEM observations since the coercive field increased with

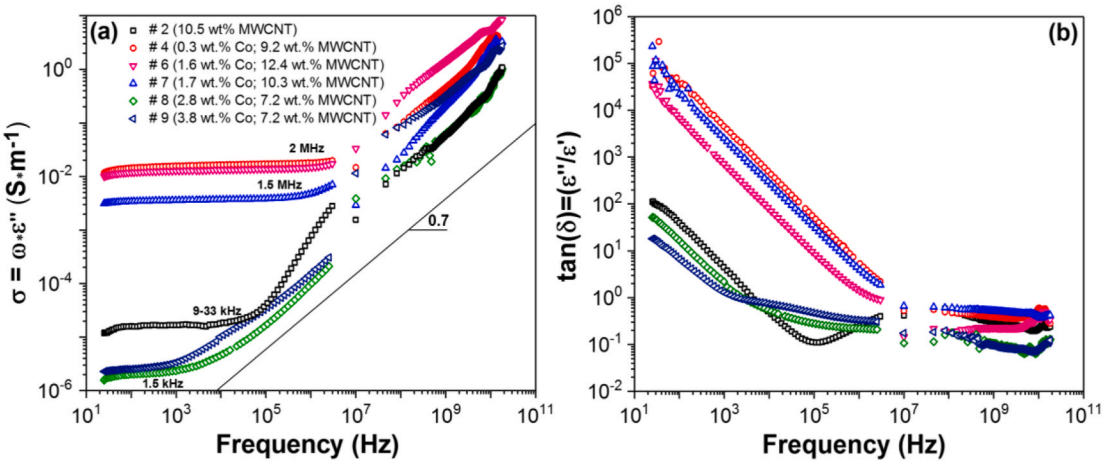

Fig. 5. Frequency dispersion of the dielectric properties of Co/MWCNT-PE composites depending on the content of Co and MWCNT in samples. (a) - AC electrical conductivity; (b) - loss tangent. The thickness of all the samples was about 0.5 mm. For the conductivity, the cross-over frequency between a constant and a 0.7 power-law is reported on the graph.

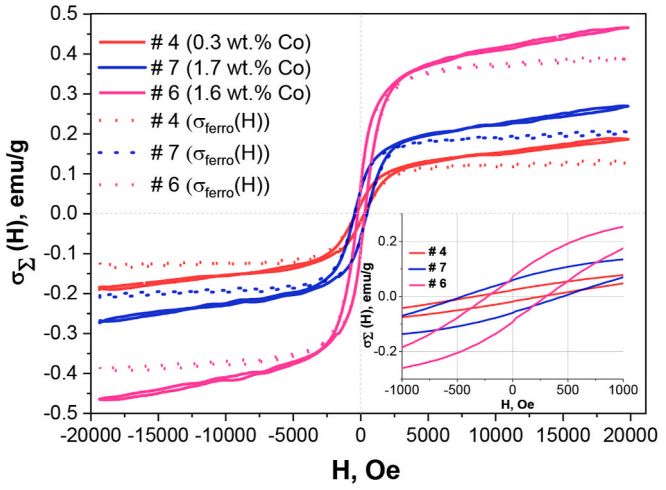

Fig. 6. Magnetic hysteresis loops of Co/MWCNT-PE composites: (#4 (9.5% (**3.5%** Co/MWCNT)-PE); #7 (12% (**14.5%** Co/MWCNT)-PE), and #6 (14% (**11.7%** Co/MWCNT)-PE)) with maximum applied magnetic field ± 20 kOe at 300 K. Solid lines are measured magnetization values (σ_Σ (H)), while dotted lines are the ferromagnetic contributions ($\sigma_{ferro}(H)$) obtained after subtraction of the susceptibility of the paraprocess (Eq. (3)); the inset shows the details of the magnetic hysteresis loops with an applied field of 1 KOe. The magnetization is expressed by mass of sample.

Table 2
Comparison of Co content, average particle sizes observed by HRTEM, and magnetic parameters (coercive field, saturation magnetization, remanence ratio and paramagnetic susceptibility) measured on three Co/MWCNT-PE composites with various Co:MWCNT:PE ratios derived from the data of Fig. 7 and re-expressed by mass of Co in the samples.

# Sample	Co loading, (wt.%)	Mean Co size (nm)	H_C, (Oe)	σ_S (emu/g)	σ_r/σ_S	$\chi_{para}*10^6$ (g/cm^3)
4	0.3	4	125	36	0.25	3.5
6	1.6	14	243	23	0.2	5.0
7	1.7	20	339	10	0.5	4.5

particle size. However, the saturation magnetization σ_S decreased when it was expected to increase with particle sizes since, in larger particles, surface effects become less important and the value is expected to approach the one of the bulk (162.5 emu.g^{-1}). This did not happen though. This might be due to differences in surface states for the particles inside the MWCNT observed in sample #4 with respect to the larger particles outside the MWCNT which represents the majority of Co nanoparticles in sample #7. In that respect, the appearance of the para process was equally revealing as it also reflected the heterogeneity of the nanoparticles (Note that the susceptibility values observed here for the para process were reasonably close to the high field susceptibility of bulk Co, $4.50{\cdot}10^{-6}$ emu.g^{-1}.Oe^{-1}). It was the signature not only of the presence of very small (below 5 nm) [21] Co nanoparticles in a superparamagnetic state but possibly also of a defective surface layer at the surface of larger Co nanoparticles. Indeed, for all samples of the series # 4–9, a population of Co elongated nanoparticles located inside the channels of the MWCNTs was observed by HRTEM (Fig. S1) but its relative importance decreased with Co loading. Significantly, this translated in a modification of the remanence ratio which went from the expected value of 0.5 for spherical hcp Co particles in sample #7 to a smaller value of 0.2 for sample #4 indicative of a deviation from sphericity. In summary, the magnetic characterization of the overall samples confirmed and complemented the locally restricted information obtained by HRTEM.

Ferromagnetic Resonance (FMR) method was used to further evaluate the high-frequency magnetic properties of the Co/MWCNT-PE composites. The experimental FMR curves for Co/MWCNT-PE composites with various component ratios measured at the frequency of 50 GHz are shown in Fig. 7.

The FMR curves for Co/MWCNT-PE composites with various component ratios were modeled within the approximation of noninteracting grains with cubic magnetocrystalline anisotropy. The noise on the experimental resonance curves reflected the low intensity of the FMR signal due to the small number of magnetic particles within the samples (the imaginary part of the relative permeability was only $\sim 10^{-3}$). These low intensities revealed the baseline distortions due to interactions of the large magnetizing field with the experimental setup (microwave generator and detector). These distortions resulted in differences between modeled and experimental baselines. From the magnetization obtained by VSM at 20 kOe (Fig. 6) and the bulk density of the Co/MWCNT-PE composite, one gets the volumetric saturation magnetization $Ms = \sigma_{20\ kOe}{\cdot}\rho$ required to calculate the components of the permeability tensor and model the FMR response at different frequencies. In this way, one obtains the values of the gyromagnetic ratios ($\gamma/2\pi$), of the effective anisotropy fields (H_a), and of the damping constant (α) of an individual grain in the Landau-Lifshitz-Hilbert equation. The bulk density of Co/MWCNT-PE composites was measured

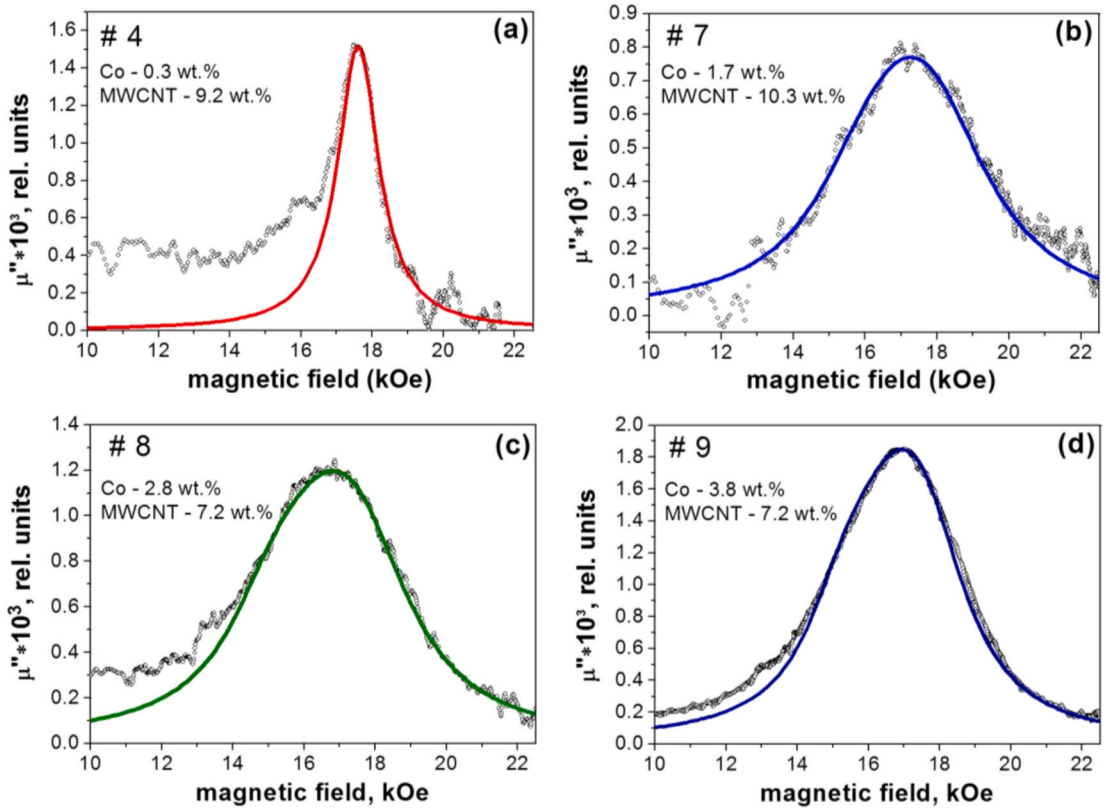

Fig. 7. Experimental (grey dots) and calculated (solid lines) FMR curves of the # 4–9 Co/MWCNT-PE composite samples with various Co:MWCNT:PE ratios. The measurement frequency was 50 GHz.

independently and varied from 0.914 to 1.171 g/cm^3 depending on the composition and Co:MWCNT:PE ratios. The values of saturation magnetizations, gyromagnetic ratios, anisotropy fields and damping constant are given in Table 3.

The obtained value of the gyromagnetic ratio for samples #4 was close to the gyromagnetic ratio for the spin of a free electron (2.8 GHz/kOe). The gyromagnetic ratio then increased with increasing content of cobalt. This was a reflection of an increased size of the cobalt particles. In effect, increasing the Co loading led to a decreased proportion of smaller Co nanoparticles in a superparamagnetic and/or amorphous state. The relative contribution arising from the defective surface layer of Co nanoparticles was also reduced. The particle size growth, caused by the Co content increase in the samples, resulted in the formation of Co nanoparticles of properties closer to the ones of bulk cobalt particle ($\gamma/2\pi = 3.15$ GHz/kOe), in line with the analysis of the static magnetization hysteresis loop reported above.

The magnitude of the effective anisotropy field H_a was about 2 kOe and the damping constant about 0.1 except for sample #4. In that sample, the nanoparticles thus exhibited for a large part a behavior close to magnetocrystalline anisotropy and reduced grain heterogeneity in line with HRTEM observations. However, for the sample # 4, the fit quality was poor compared to the ones of the other samples. Most probably this sample was biphasic, i.e. it contained both magnetically soft and hard phases. The almost null anisotropy field in that sample was due to a significant part of Co being in a superparamagnetic state (magnetically soft). A similar sample was thoroughly studied in Ref. [21] by means of internal field NMR but this method provides a signal originating solely from the magnetically hard phase, i.e. the Co nanoparticles whose ferromagnetism is either stabilized by Co and MWCNT specific interaction, or due to a high aspect ratio (oblong Co nanoparticles and sometimes even short nanowires were observed inside of the MWCNT channels by HRTEM).

Table 3
FMR parameters (magnetization saturation per unit volume, effective anisotropy field, gyromagnetic ratio and damping constant) for Co/MWCNT-PE composites with various component ratios. The mean Co nanoparticle sizes obtained by HRTEM are also reported for comparison sake.

# Sample	Co loading (wt.%)	Mean Co size (nm)	M_S (emu/cm^3)	H_a (kOe)	$\gamma/2\pi$ (GHz/kOe)	α
4	0.3	4	0.17	0.0 ± 0.2	2.84 ± 0.02	0.04 ± 0.01
7	1.7	20	0.27	1.8 ± 0.2	2.89 ± 0.02	0.11 ± 0.01
8	2.8	24	0.41	2.2 ± 0.2	2.98 ± 0.02	0.10 ± 0.01
9	3.8	45	0.53	2.0 ± 0.2	2.97 ± 0.02	0.08 ± 0.01

Finally, the complex permeability (μ', μ") of the Co/MWCNT-PE composites were measured in the frequency range of 10 MHz–18 GHz together with the permittivity already discussed in section 3.3 (Fig. 5). The real (μ') and the imaginary (μ") parts of the complex permeability of the Co/MWCNT-PE composite samples as a function of frequency are shown in Fig. 8 (a) and (b), respectively.

For the MWCNT-PE samples, they were very low in the whole 10 MHz−18 GHz frequency range due to the weak magnetic characteristic of PE and MWCNT materials and thus not reported here. The samples containing Co on the other hands exhibited significant values of μ' and μ" which varied with MWCNT loadings, Co loadings and thus Co nanoparticles size (since it depended on the loading as shown by HRTEM). The fluctuating part in the permeability curves of the composite at lower frequency (2–10 GHz) is attributed to resonance peaks, which may be caused by natural ferromagnetic resonance, domain wall resonance or eddy current effect [34]. In the polymeric composite filled with magnetic particles, the magnetic losses are preferably controlled by the natural ferromagnetic resonance, exchange resonance and Foucault

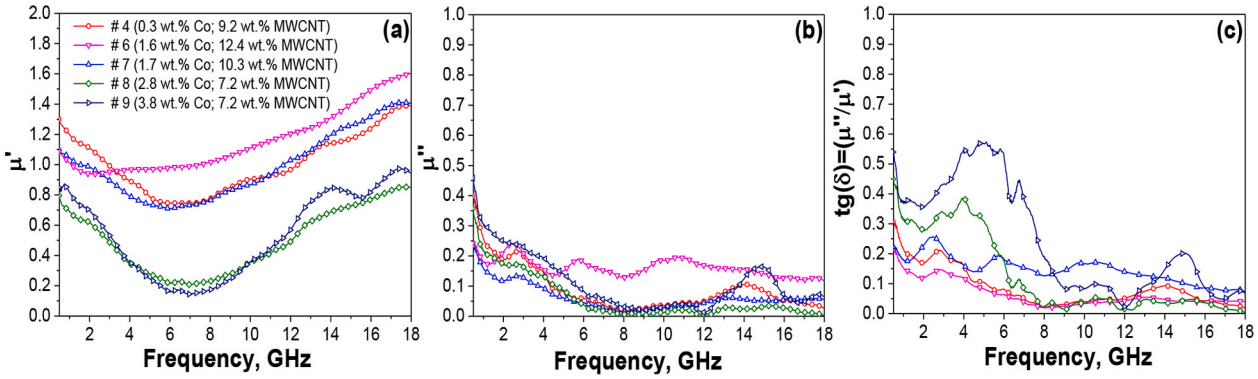

Fig. 8. The real part (a) and the imaginary part (b) of complex permeability and magnetic loss (c) for the Co/MWCNT-PE composites with various components loading at 10 MHz–18 GHz.

current effect along with the domain wall resonance, magnetic hysteresis and space charge polarization [35]. In the cobalt particles, the natural ferromagnetic resonance and exchange resonance coexist, which can also be attributed to the magnetic loss [36]. In the frequency range of 2–8 GHz, a region of natural ferromagnetic resonance for Co/MWCNT-PE samples was observed (Fig. 8 a-b). This resonance was evidenced by the resonant behavior of the real part μ' (transition through unity) and the occurrence of local maxima for the imaginary part μ". It is known [37] that for a cubic crystal structure, the frequency of natural ferromagnetic resonance (ω_{nr}) can be defined as $\omega_{nr} = \frac{2}{3}\gamma H_a$. From the FMR data, the anisotropy field was about 2 kOe and the gyromagnetic ratio about 2 GHz/kOe (Table 3). Consequently, the frequency of natural ferromagnetic resonance for Co/MWCNT-PE samples was thus expected around 4 GHz. This value was consistent to the aforementioned observed resonant features of the permeability dispersion in the 2–8 GHz range. The increase of the cobalt loading as well as the concomitant Co particles size (from 4 to 45 nm), led to an overall increase in the imaginary part of the magnetic permeability in the frequency range up to 1 GHz, a fact that was related to the increase of the saturation magnetization seen in Fig. 6. Sample # 6 had higher magnetic losses than the other samples apparently due to the joint interaction of the magnetic component and the currents excited in the carbon nanotubes.

3.5. Reflection losses of Co/MWCNT-PE composites

According to the transmission line theory [38], in order to obtain the desired impedance match, ε should be close to μ for absorbers materials. By varying the content of Co nanoparticles and MWCNT in the polyethylene matrix, and thus the complex permeability of composites, one can thus expect to optimize the electromagnetic wave absorption of the material. In that respect, the electromagnetic absorption of

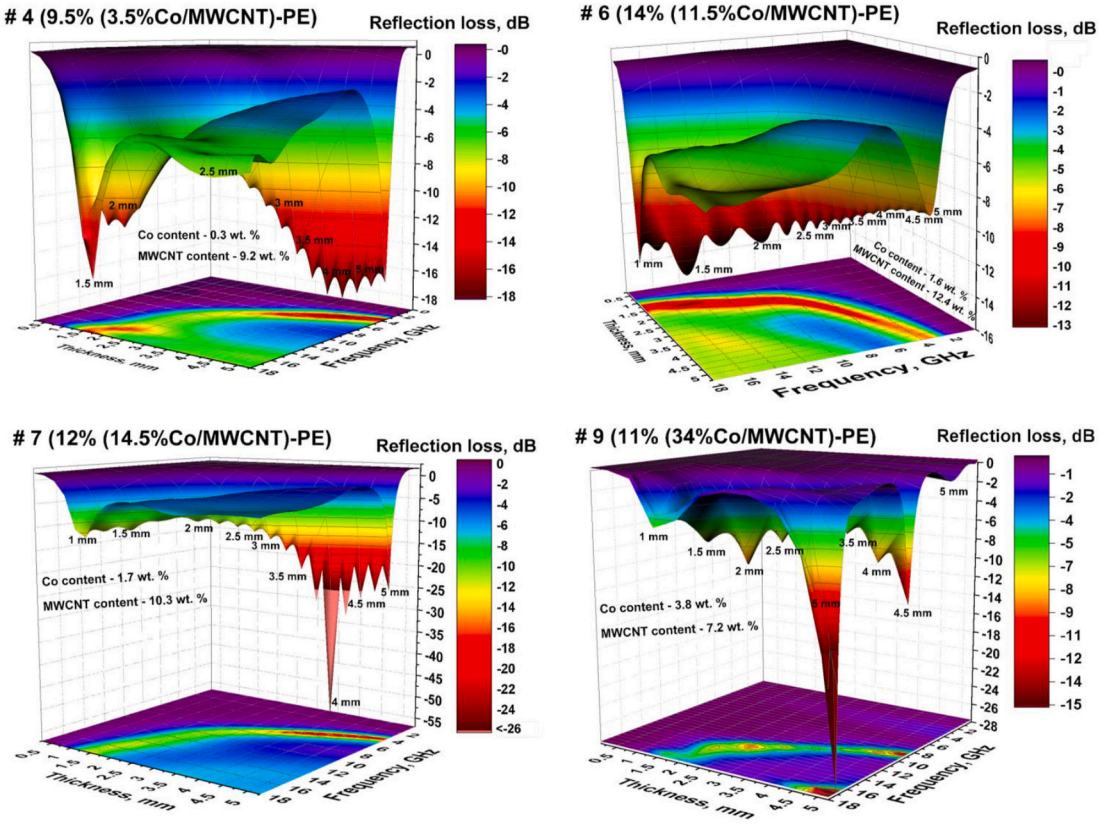

Fig. 9. Frequency dependences of reflection loss for Co/MWCNT-PE composites with various components loading at with 0.1–5 mm of thickness at 10 MHz–18 GHz.

Co/MWCNT-PE composites depending on the Co:MWCNT:PE ratios was evaluated by calculating the refection loss (RL) through equations (2) and (3). Fig. 9 shows the calculated RL of Co/MWCNT-PE composites with various Co:MWCNT:PE ratios and with different thicknesses.

For all samples, as expected, the microwave absorption peaks shifted to lower frequency position when the coating thickness increased from 0.1 mm to 5 mm. The microwave absorption properties closely correspond to the magnetic loss, dielectric loss and impedance matching between complex permittivity and complex permeability. The reflection loss characteristics of the samples #4, #6, #7 and #9 are summarized in Table S2. For instance, one can examine how these composites behave with regards to two common frequency bands: 5 GHz (used for Wi-Fi) and 2 GHz (used for mobile telephones). The composite material # 7 (1.7 wt% Co; 10.3 wt% MWCNT) with a thickness of 4 mm attenuated the signal in the 5 GHz region by approximately 5 orders of magnitude. At the same time, in the area of 2 GHz and lower frequency range, the efficiency of attenuation of electromagnetic radiation for this composite material was quite low. This exemplifies how these materials can be used to shield one frequency band without interfering with the other.

4. Discussion

For all the composites for which the reflective losses were evaluated, the stronger absorption around 4–5 GHz could be ascribed to the relatively high dielectric loss and the enhancement of permeability and magnetic loss. Consider for example sample # 7. For the composite film thickness of 1.5 mm, this sample has the best high frequency microwave absorption in the frequency range of 12.8–17.8 GHz. This sample indeed had the higher permeability (Fig. 8), relatively strong magnetic loss and excellent impedance matching. This demonstrated how the RL could be tuned to target by varying the Co and MWCNT content of the PE composites.

To comprehensively evaluate the effectiveness of the obtained Co/MWCNT-PE composite, we compared the reflection loss properties of state-of-the-art absorbers based on polymer composites containing magnetic nanoparticles and carbon nanostructured materials (Table S3, Fig. 10). Looking at the data reported in Table S3, it is clear that the majority of the composite materials listed there are based on a paraffin matrix. However, the use of paraffin limits the practical use of such composites due to its low melting point (45–65 °C) and low mechanical strength. On the contrary, the material presented in this work is based on polyethylene which has a much higher melting point (136–140 °C) (see Table S1 and Fig. S6). Also, it should be noted that the use of carbon nanotubes in comparison with other carbon nanomaterials provides better absorption properties at a lower total filler loading: the values of the present samples reported in Table 1 and reproduced for comparison at the end of Table S3 classifying them definitely among the lower carbon content samples.

It could thus be concluded that following the synthetic proposed here, it was possible to achieve similar reflection loss and effective bandwidth (RL < −10 dB) (Table S3, Fig. 10(a–b)) than other composites containing magnetic nanoparticles and carbon nanostructured materials but at lower total filler loading. This is even more striking when comparing the specific reflection losses relative to the total filler loading

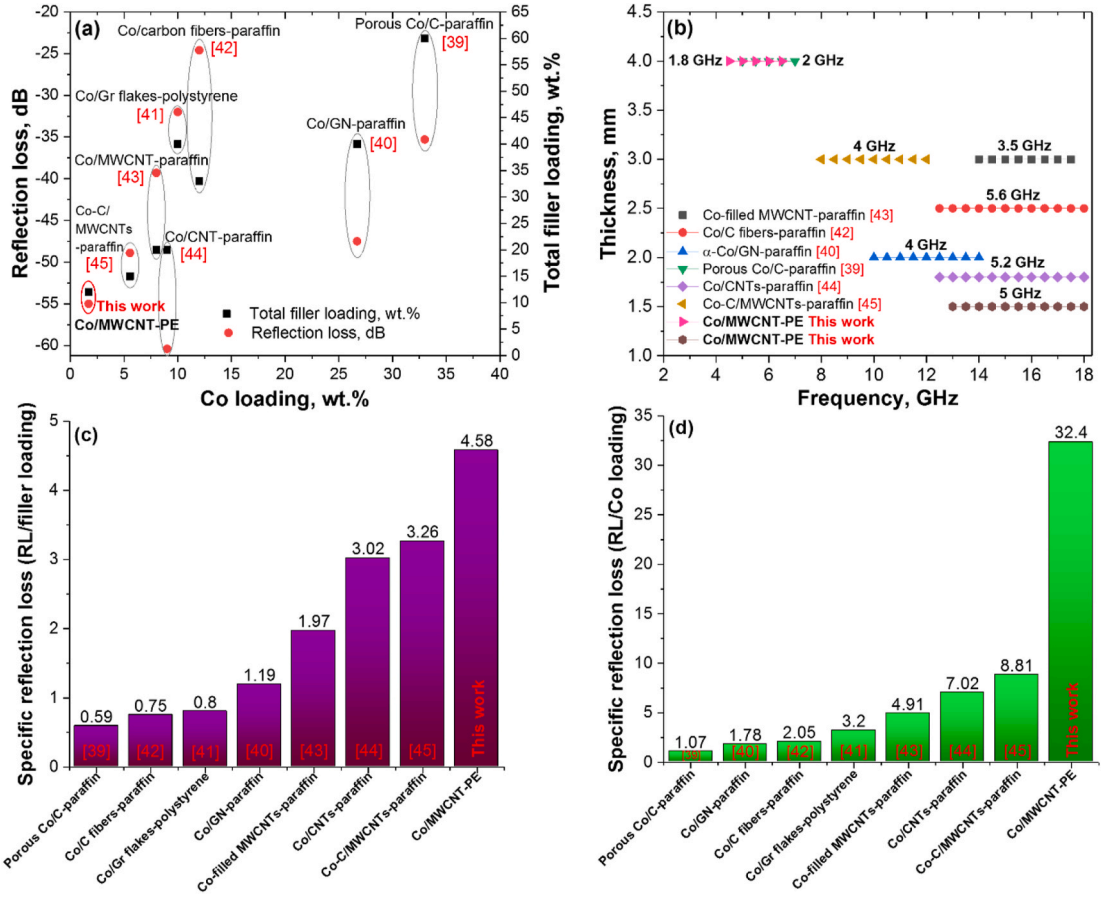

Fig. 10. (a) Minimum reflection loss versus the total loading of filler and Co nanoparticles in the composites obtained in this work compared with previously reported composites [39–45] containing Co nanoparticles and nanostructured carbon materials. (b) Comparison of the effective bandwidths (RL < 10 dB) of recently reported polymer composites with varying thicknesses. Comparison of specific reflection loss relative to the total filler loading (RL/filler loading) (c) and to Co loading (RL/Co loading) (d) for Co/MWCNT-PE composites obtained in this work and previously studied absorbers based on Co nanoparticles and nanostructured carbon materials.

(Fig. 10 (c)) or to the Co loading (Fig. 10 (d)). The polyethylene composites synthesized in the present study demonstrated significantly better characteristics than other absorbers with a similar composition.

Finally, Co/MWCNT-PE composites are obtained based on thermoplastic and commercially available polymer matrix (polyethylene) that provides cost-effective, lightweight and flexible coatings of a given shape for highly efficient shielding of electromagnetic radiation, which is undoubtedly attractive from both an environmental and economic standpoint. Clearly, such high absorption efficiency of composites were achieved thanks to the *in situ* polymerization technique that allows high dispersion of Co/MWCNT in the matrix of polyethylene. In addition, this work demonstrated that the absorption properties of Co/MWCNT-PE composites can be controlled over a wide range of EMI frequencies (2–18 GHz) by adjusting both the content of magnetic, dielectric components and the thickness of the composite. Thus, in this study, a unique approach was used to obtain composite materials capable of effective reduction of electromagnetic radiation through synergistic effect of Co and MWCNT in a commercially available polymer matrix.

5. Conclusions

A set of Co/MWCNT loaded PE composites with varying composition has been successfully prepared via *in situ* polymerization of ethylene with the Ti-Ziegler–Natta catalyst preliminarily immobilized on Co/MWCNT hybrids. Co/MWCNT hybrids with various Co loading and different Co nanoparticles size (4–45 nm) and distribution in the MWCNT structure (inside and outside of the channels) were synthesized by incipient wetness impregnation followed by reduction. The uniform distribution of the Co/MWCNT hybrids into the PE matrix has been established by the SEM and TEM images of the composite samples. The presence of the Co metal nanoparticles into PE based composites has been identified from the XRD results. The magnetic hysteresis loops and FMR spectra for Co/MWCNT-PE composites indicated a superparamagnetic feature caused by the presence of Co nanoparticles. The proportion of Co nanoparticles in a superparamagnetic state decreased with an increased Co loading and an increase of the Co nanoparticle size. The Co/MWCNT-PE composite (1.7 wt% of Co; 10.3 wt% of MWCNT) had much higher shielding effectiveness. For a thickness of 4 mm, the matching was optimum with a maximum reflection loss of −55 dB at 5.2 GHz. For a thickness of 1.5 mm, the same composite film had the largest bandwidth (RL below −10 dB in the frequency range of 12.8–17.8 GHz). Importantly, the excellent shielding efficiency of electromagnetic radiation was achieved with a total filler and Co loading of only 12 and 1.7 wt%, respectively, values that are significantly lower than that in previously studied polymer composite absorbers based on magnetic nanoparticles and nanostructured carbon materials. Thus, the Co/MWCNT-PE composite materials, combining the magnetic properties of Co, the electric ones of MWCNTs, and the mechanical ones of PE, is a promising lightweight material. They have a high potential for designing devices that effectively attenuate electromagnetic radiation in a wide frequency range that can be tuned by the sample composition and thickness.

CRediT authorship contribution statement

Mariya A. Kazakova: Investigation, Conceptualization, Writing – original draft, Writing – review & editing. **Nina V. Semikolenova:** Investigation, Methodology. **Evgeniy Yu. Korovin:** Investigation. **Viktor A. Zhuravlev:** Investigation, Validation. **Alexander G. Selyutin:** Investigation, Visualization. **Dmitry A. Velikanov:** Investigation. **Sergey I. Moseenkov:** Investigation. **Andrey S. Andreev:** Conceptualization. **Olga B. Lapina:** Validation, Writing – review & editing. **Valentin I. Suslyaev:** Conceptualization, Writing – review & editing. **Mikhail A. Matsko:** Conceptualization, Writing – review & editing. **Vladimir A. Zakharov:** Conceptualization. **Jean-Baptiste d'Espinose de Lacaillerie:** Conceptualization, Writing – review & editing.

Declaration of competing interest

The authors declare that they have no known competing financial interests or personal relationships that could have appeared to influence the work reported in this paper.

Acknowledgements

This work was supported by the Ministry of Science and Higher Education of the Russian Federation within the state assignment for Boreskov Institute of Catalysis (project # AAAA-A21-121011390054-1).

Appendix A. Supplementary data

Supplementary data to this article can be found online at https://doi.org/10.1016/j.compscitech.2021.108731.

References

[1] F. Shahzad, M. Alhabeb, C.B. Hatter, B. Anasori, S. Man Hong, C.M. Koo, Y. Gogotsi, Electromagnetic interference shielding with 2D transition metal carbides (MXenes), Science 353 (6304) (2016) 1137, https://doi.org/10.1126/science.aag2421.

[2] Y.-J. Tan, J. Li, X.-H. Tang, T.-N. Yue, M. Wang, Effect of phase morphology and distribution of multi-walled carbon nanotubes on microwave shielding of poly(l-lactide)/poly(ε-caprolactone) composites, Compos. Part A Appl. Sci. Manuf. 137 (2020), 106008, https://doi.org/10.1016/j.compositesa.2020.106008.

[3] X.-H. Tang, J. Li, Y. Wang, Y.-X. Weng, M. Wang, Controlling distribution of multi-walled carbon nanotube on surface area of Poly(ε-caprolactone) to form sandwiched structure for high-efficiency electromagnetic interference shielding, Compos. B Eng. 196 (2020), 108121, https://doi.org/10.1016/j.compositesb.2020.108121.

[4] X.-H. Tang, Y. Tang, Y. Wang, Y.-X. Weng, M. Wang, Interfacial metallization in segregated poly (lactic acid)/poly (ε-caprolactone)/multi-walled carbon nanotubes composites for enhancing electromagnetic interference shielding, Compos. Part A Appl. Sci. Manuf. 139 (2020), 106116, https://doi.org/10.1016/j.compositesa.2020.106116.

[5] T. Wang, W.-C. Yu, W.-J. Sun, L.-C. Jia, J.-F. Gao, J.-H. Tang, H.-J. Su, D.-X. Yan, Z.-M. Li, Healable polyurethane/carbon nanotube composite with segregated structure for efficient electromagnetic interference shielding, Compos. Sci. Technol. 200 (2020), 108446, https://doi.org/10.1016/j.compscitech.2020.108446.

[6] Y.L. Xu, A. Uddin, D. Estevez, Y. Luo, H.X. Peng, F.X. Qin, Lightweight microwire/graphene/silicone rubber composites for efficient electromagnetic interference shielding and low microwave reflectivity, Compos. Sci. Technol. 189 (2020), 108022, https://doi.org/10.1016/j.compscitech.2020.108022.

[7] S.P. Pawar, G. Melo, U. Sundararaj, Dual functionality of hierarchical hybrid networks of multiwall carbon nanotubes anchored magnetite particles in soft polymer nanocomposites: simultaneous enhancement in charge storage and microwave absorption, Compos. Sci. Technol. 183 (2019), 107802, https://doi.org/10.1016/j.compscitech.2019.107802.

[8] B. Wen, X. Wang, Y. Zhang, Ultrathin and anisotropic polyvinyl butyral/Ni-graphite/short-cut carbon fibre film with high electromagnetic shielding performance, Compos. Sci. Technol. 169 (2019) 127–134, https://doi.org/10.1016/j.compscitech.2018.11.013.

[9] P. Pötschke, S.M. Dudkin, I. Alig, Dielectric spectroscopy on melt processed polycarbonate—multiwalled carbon nanotube composites, Polymer 44 (17) (2003) 5023–5030, https://doi.org/10.1016/S0032-3861(03)00451-8.

[10] C. Wang, V. Murugadoss, J. Kong, Z. He, X. Mai, Q. Shao, Y. Chen, L. Guo, C. Liu, S. Angaiah, Z. Guo, Overview of carbon nanostructures and nanocomposites for electromagnetic wave shielding, Carbon 140 (2018) 696–733, https://doi.org/10.1016/j.carbon.2018.09.006.

[11] J.-H. Cai, J. Li, X.-D. Chen, M. Wang, Multifunctional polydimethylsiloxane foam with multi-walled carbon nanotube and thermo-expandable microsphere for temperature sensing, microwave shielding and piezoresistive sensor, Chem. Eng. J. (Lausanne) 393 (2020), 124805, https://doi.org/10.1016/j.cej.2020.124805.

[12] J. Ju, T. Kuang, X. Ke, M. Zeng, Z. Chen, S. Zhang, X. Peng, Lightweight multifunctional polypropylene/carbon nanotubes/carbon black nanocomposite foams with segregated structure, ultralow percolation threshold and enhanced electromagnetic interference shielding performance, Compos. Sci. Technol. 193 (2020), 108116, https://doi.org/10.1016/j.compscitech.2020.108116.

[13] Y. Chen, P. Pötschke, J. Pionteck, B. Voit, H. Qi, Multifunctional cellulose/rGO/Fe_3O_4 composite aerogels for electromagnetic interference shielding, ACS Appl. Mater. Interfaces 12 (19) (2020) 22088–22098, https://doi.org/10.1021/acsami.9b23052.

[14] Y. Fei, M. Liang, L. Yan, Y. Chen, H. Zou, Co/C@cellulose nanofiber aerogel derived from metal-organic frameworks for highly efficient electromagnetic interference shielding, Chem. Eng. J. (Lausanne) 392 (2020), 124815, https://doi.org/10.1016/j.cej.2020.124815.

[15] L. Vazhayal, P. Wilson, K. Prabhakaran, Waste to wealth: lightweight, mechanically strong and conductive carbon aerogels from waste tissue paper for electromagnetic shielding and CO_2 adsorption, Chem. Eng. J. (Lausanne) 381 (2020), 122628, https://doi.org/10.1016/j.cej.2019.122628.
[16] N. Yang, Z.-X. Luo, G.-R. Zhu, S.-C. Chen, X.-L. Wang, G. Wu, Y.-Z. Wang, Ultralight three-dimensional hierarchical cobalt nanocrystals/N-doped CNTs/carbon sponge composites with a hollow skeleton toward superior microwave absorption, ACS Appl. Mater. Interfaces 11 (39) (2019) 35987–35998, https://doi.org/10.1021/acsami.9b11101.
[17] F.X. Qin, C. Brosseau, H.X. Peng, Microwave properties of carbon nanotube/microwire/rubber multiscale hybrid composites, Chem. Phys. Lett. 579 (2013) 40–44, https://doi.org/10.1016/j.cplett.2013.06.021.
[18] M.A. Kazakova, V.L. Kuznetsov, N.V. Semikolenova, S.I. Moseenkov, D. V. Krasnikov, M.A. Matsko, A.V. Ishchenko, V.A. Zakharov, A.I. Romanenko, O. B. Anikeeva, E.N. Tkachev, V.I. Suslyaev, V.A. Zhuravlev, K.V. Dorozkin, Comparative study of multiwalled carbon nanotube/polyethylene composites produced via different techniques, Phys. Status Solidi B 251 (12) (2014) 2437–2443, https://doi.org/10.1002/pssb.201451194.
[19] M.A. Kazakova, A.G. Selyutin, N.V. Semikolenova, A.V. Ishchenko, S.I. Moseenkov, M.A. Matsko, V.A. Zakharov, V.L. Kuznetsov, Structure of the in situ produced polyethylene based composites modified with multi-walled carbon nanotubes: in situ synchrotron X-ray diffraction and differential scanning calorimetry study, Compos. Sci. Technol. 167 (2018) 148–154, https://doi.org/10.1016/j.compscitech.2018.07.046.
[20] M.A. Kazakova, N.V. Semikolenova, E.Y. Korovin, S.I. Moseenkov, A.S. Andreev, A. S. Kachalov, V.L. Kuznetsov, V.I. Suslyaev, M.A. Mats'ko, V.A. Zakharov, In situ polymerization technique for obtaining composite materials based on polyethylene, multi-walled carbon nanotubes and cobalt nanoparticles, Russ. J. Appl. Chem. 91 (1) (2018) 127–135, https://doi.org/10.1134/S1070427218010202.
[21] A.S. Andreev, M.A. Kazakova, A.V. Ishchenko, A.G. Selyutin, O.B. Lapina, V. L. Kuznetsov, J.-B. d'Espinose de Lacaillerie, Magnetic and dielectric properties of carbon nanotubes with embedded cobalt nanoparticles, Carbon 114 (2017) 39–49, https://doi.org/10.1016/j.carbon.2016.11.070.
[22] M.A. Kazakova, A.S. Andreev, A.G. Selyutin, A.V. Ishchenko, A.V. Shuvaev, V. L. Kuznetsov, O.B. Lapina, J.-B. d'Espinose de Lacaillerie, Co metal nanoparticles deposition inside or outside multi-walled carbon nanotubes via facile support pretreatment, Appl. Surf. Sci. 456 (2018) 657–665, https://doi.org/10.1016/j.apsusc.2018.06.124.
[23] F. Ma, Y. Qin, Y.-Z. Li, Enhanced microwave performance of cobalt nanoflakes with strong shape anisotropy, Appl. Phys. Lett. 96 (20) (2010), 202507, https://doi.org/10.1063/1.3432441.
[24] V.F. Puntes, K.M. Krishnan, A.P. Alivisatos, Colloidal nanocrystal shape and size control: the case of cobalt, Science 291 (5511) (2001) 2115–2117, https://doi.org/10.1126/science.1058495.
[25] G.V. Golubtsov, M.A. Kazakova, A.G. Selyutin, A.V. Ishchenko, V.L. Kuznetsov, Mono-, Bi-, and trimetallic catalysts for the synthesis of multiwalled carbon nanotubes based on iron subgroup metals, J. Struct. Chem. 61 (4) (2020) 640–651, https://doi.org/10.1134/S0022476620040186.
[26] M.A. Kazakova, D.M. Morales, C. Andronescu, K. Elumeeva, A.G. Selyutin, A. V. Ishchenko, G.V. Golubtsov, S. Dieckhöfer, W. Schuhmann, J. Masa, Fe/Co/Ni mixed oxide nanoparticles supported on oxidized multi-walled carbon nanotubes as electrocatalysts for the oxygen reduction and the oxygen evolution reactions in alkaline media, Catal. Today 357 (2020) 259–268, https://doi.org/10.1016/j.cattod.2019.02.047.
[27] M.A. Kazakova, A.G. Selyutin, A.V. Ishchenko, A.S. Lisitsyn, K.Y. Koltunov, V. I. Sobolev, Co/multi-walled carbon nanotubes as highly efficient catalytic nanoreactor for hydrogen production from formic acid, Int. J. Hydrogen Energy 45 (38) (2020) 19420–19430, https://doi.org/10.1016/j.ijhydene.2020.05.127.
[28] A.A. Zhdanov, M.A. Kazakova, Use of carbon materials with various nature in determining the content of metals in carbon nanotubes by the X-ray fluorescence method, J. Anal. Chem. 75 (3) (2020) 312–319, https://doi.org/10.1134/S106193482003017X.
[29] M.A. Kazakova, E.Y. Korovin, S.I. Moseenkov, A.S. Kachalov, D.I. Sergeenko, A. V. Shuvaev, V.L. Kuznetsov, V.I. Suslyaev, Electromagnetic parameters of composite materials based on polyethylene and multi-walled carbon nanotubes modified by iron oxide nanoparticles, Russ. J. Appl. Chem. 91 (12) (2018) 1994–2002, https://doi.org/10.1134/S107042721812011X.
[30] M.A. Kazakova, S.I. Moseenkov, G.V. Golubtsov, E.Y. Korovin, A.V. Ishchenko, A. G. Selyutin, A.V. Zavorin, V.A. Zhuravlev, V.I. Suslyaev, V.L. Kuznetsov, Structural and electromagnetic properties of Fe_2Co-multi-walled carbon nanotubes-polystyrene based composite, J. Alloys Compd. 844 (2020), 156107, https://doi.org/10.1016/j.jallcom.2020.156107.
[31] J.P. Clerc, G. Giraud, J.M. Laugier, J.M. Luck, The electrical conductivity of binary disordered systems, percolation clusters, fractals and related models, Adv. Phys. 39 (3) (1990) 191–309, https://doi.org/10.1080/00018739000101501.
[32] Z. Yu, Z. Yao, N. Zhang, Z. Jiang, Polarization enhanced multi-grain-boundary dendritic micro–nano structure α-Fe for electromagnetic absorption applications: synthesis and characterization, RSC Adv. 5 (32) (2015) 25266–25272, https://doi.org/10.1039/C5RA01665G.
[33] Z. Wang, H. Bi, P. Wang, M. Wang, Z. Liu, L. shen, X. Liu, Magnetic and microwave absorption properties of self-assemblies composed of core–shell cobalt–cobalt oxide nanocrystals, Phys. Chem. Chem. Phys. 17 (5) (2015) 3796–3801, https://doi.org/10.1039/C4CP04985C.
[34] M. Cao, C. Han, X. Wang, M. Zhang, Y. Zhang, J. Shu, H. Yang, X. Fang, J. Yuan, Graphene nanohybrids: excellent electromagnetic properties for the absorbing and shielding of electromagnetic waves, J. Mater. Chem. C 6 (17) (2018) 4586–4602, https://doi.org/10.1039/C7TC05869A.
[35] A. Ansari, M.J. Akhtar, Investigation on electromagnetic characteristics, microwave absorption, thermal and mechanical properties of ferromagnetic cobalt–polystyrene composites in the X-band (8.4–12.4 GHz), RSC Adv. 6 (17) (2016) 13846–13857, https://doi.org/10.1039/C5RA26489H.
[36] H. Wang, N. Ma, Z. Yan, L. Deng, J. He, Y. Hou, Y. Jiang, G. Yu, Cobalt/polypyrrole nanocomposites with controllable electromagnetic properties, Nanoscale 7 (16) (2015) 7189–7196, https://doi.org/10.1039/C4NR06978A.
[37] A.G. Gurevich, G.A. Melkov, Magnetization Oscillations and Waves, CRC Press, 1996.
[38] D. Zhang, F. Xu, J. Lin, Z. Yang, M. Zhang, Electromagnetic characteristics and microwave absorption properties of carbon-encapsulated cobalt nanoparticles in 2–18-GHz frequency range, Carbon 80 (Supplement C) (2014) 103–111, https://doi.org/10.1016/j.carbon.2014.08.044.
[39] A. Ansari, M.J. Akhtar, Co/graphite based light weight microwave absorber for electromagnetic shielding and stealth applications, Mater. Res. Express 4 (1) (2017), 016304, https://doi.org/10.1088/2053-1591/aa570c.
[40] W. Li, H. Qi, F. Guo, Y. Du, N. Song, Y. Liu, Y. Chen, Co nanoparticles supported on cotton-based carbon fibers: a novel broadband microwave absorbent, J. Alloys Compd. 772 (2019) 760–769, https://doi.org/10.1016/j.jallcom.2018.09.075.
[41] H. Lin, H. Zhu, H. Guo, L. Yu, Microwave-absorbing properties of Co-filled carbon nanotubes, Mater. Res. Bull. 43 (10) (2008) 2697–2702, https://doi.org/10.1016/j.materresbull.2007.10.016.
[42] Y. Lü, Y. Wang, H. Li, Y. Lin, Z. Jiang, Z. Xie, Q. Kuang, L. Zheng, MOF-derived porous Co/C nanocomposites with excellent electromagnetic wave absorption properties, ACS Appl. Mater. Interfaces 7 (24) (2015) 13604–13611, https://doi.org/10.1021/acsami.5b03177.
[43] G. Pan, J. Zhu, S. Ma, G. Sun, X. Yang, Enhancing the electromagnetic performance of Co through the phase-controlled synthesis of hexagonal and cubic Co nanocrystals grown on graphene, ACS Appl. Mater. Interfaces 5 (23) (2013) 12716–12724, https://doi.org/10.1021/am404117v.
[44] Y. Yin, X. Liu, X. Wei, Y. Li, X. Nie, R. Yu, J. Shui, Magnetically aligned Co–C/MWCNTs composite derived from MWCNT-interconnected zeolitic imidazolate frameworks for a lightweight and highly efficient electromagnetic wave absorber, ACS Appl. Mater. Interfaces 9 (36) (2017) 30850–30861, https://doi.org/10.1021/acsami.7b10067.
[45] Y. Yin, X. Liu, X. Wei, R. Yu, J. Shui, Porous CNTs/Co composite derived from zeolitic imidazolate framework: a lightweight, ultrathin, and highly efficient electromagnetic wave absorber, ACS Appl. Mater. Interfaces 8 (50) (2016) 34686–34698, https://doi.org/10.1021/acsami.6b12178.